Characterization of overlapping betatron resonances above the phase advance of 90° per cell

K. Kojima and H. Okamoto[*]

Graduate School of Advanced Science and Engineering, Hiroshima University, 1-3-1 Kagamiyama, Higashi-Hiroshima 739-8530, Japan

(Received 13 August 2021; accepted 3 February 2022; published 28 February 2022)

The space-charge-induced resonance band just above the betatron phase advance of 90° per cell is of great practical importance. The instability is closely related to the linear collective mode and can thus give rise to severe emittance growth at high beam density. In a circular machine, this type of second-order resonance occurs not only at half-integer tunes but also near quarter-integer tunes, depending on the lattice superperiodicity. Self-consistent numerical simulations are carried out to elucidate the resonance feature above the 90° cell tune. The present results suggest the existence of three different resonance mechanisms working there; namely, the fourth-order *incoherent* resonance in the beam tail, the second-order and fourth-order *coherent* resonances in the beam core. It is reconfirmed that no serious emittance growth occurs even if particles deep inside the core satisfy the incoherent resonance condition. The recently proposed *stop-band diagram*, free from the concept of incoherent tune spread, appears to be consistent with the numerical observations.

DOI: 10.1103/PhysRevAccelBeams.25.024201

I. INTRODUCTION

Owing to the recent progress of accelerator technologies, the performance of high-intensity hadron machines is getting better and better. For instance, it is now possible to accelerate a megawatt-class high-power proton beam with very low particle losses of the order of 0.1% [1]. Future hadron machines will aim at even more challenging goals, which makes it vital to take various space-charge-induced effects carefully into account in their conceptual design stages. It is particularly important to establish a basic understanding of collective resonances.

As the Coulomb interaction reaches a long distance, individual particles forming a dense beam core cannot move independently. Even if the beam intensity is low, the space-charge interaction is known to seriously affect the performance of an advanced cooler storage ring where the beam is strongly compressed in phase space [2]. The most popular approach to such space-charge issues is the use of self-consistent simulation codes, though reliable long-term simulations still need a considerable amount of CPU time. Compact non-neutral plasma trap systems can also provide a powerful means for an experimental investigation of intense beam behavior in alternating-gradient (AG) lattices [3–7].

Modern particle accelerators rely on the principle of strong focusing almost without exception [8,9]. Discrete focusing elements, generally quadrupole magnets, are aligned along the beam orbit to confine relativistic charged particles in the transverse dimensions. When the design orbit is closed as in a synchrotron, the beam receives periodic driving forces from the magnets every turn and thus loses its stability due to resonance under a specific condition. In the case of noncoupling resonance that occurs in either the horizontal or vertical direction, the single-particle resonance condition is given by $m\nu_0 = n$ where ν_0 is the betatron tune, m represents the order of the driving field, and n is an integer [10,11]. Resonance of lower order is usually stronger. Gradient errors in the quadrupole magnets lead to the harmful linear ($m = 2$) instability that is often called "half-integer resonance" because the corresponding resonance condition can be written as $\nu_0 = n/2$.

At high beam density, the dangerous linear parametric resonance driven by the Coulomb self-field (SF) potential can be excited near quarter integer tunes. This effect, sometimes referred to as *envelope instability*, has been discussed by many researchers mostly with linear transport designs in mind [12–18]. A detailed experimental study of the quarter-integer stop band was performed in the heavy-ion linac at the GSI, pointing out the role of the fourth-order resonance dominating over the envelope instability [19,20]. The concept of the coherent linear resonance has been used also for the designs of some high-intensity storage rings [21–23].

[*]Corresponding author.
okamoto@sci.hiroshima-u.ac.jp

A great deal of experimental effort was once put into observing the linear coherent effect at the Heavy Ion Medical Accelerator in Chiba (HIMAC) [24,25]. Since the HIMAC structure has even symmetry (the lattice superperiodicity is six), the linear parametric resonance is expected at half-integer tunes. In a ring of odd symmetry, such as the hadron synchrotrons at the Japan Proton Accelerator Research Complex (J-PARC) [1,26], the severe SF-driven instability of the linear coherent mode may take place near quarter-integer tunes as opposed to the conventional incoherent picture that only predicts weak fourth-order resonances there. The improvement of accelerator performance these days has raised the possibility that not only linear but also even nonlinear coherent parametric instabilities may play a certain role in circular machines [27–29].

A recent simulation study has concluded that there are basically two different types of resonances near the bare betatron phase advance of 90° per AG cell [30]; one is the second-order coherent parametric resonance and the other fourth-order incoherent resonances activated in the beam core as well as in the beam tail. In the following, we put an essentially different interpretation on this important resonance overlapping issue. We shall show that not two but three different types of resonances should be present slightly above a quarter-integer cell tune. Coasting beams are assumed throughout this theoretical study to concentrate upon the stability of the transverse betatron motion. As the main purpose of the paper is the characterization of overlapping resonances around an envelope-instability band, we consider a sequence of focusing-defocusing (FD) cells for simplicity instead of complex AG lattices.

The paper is organized as follows. In Sec. II, we give an overview of the resonance stop-band diagram recently proposed to spot the best machine working area in the betatron tune space [27,29]. A simple measure is then introduced in Sec. III to identify particles belonging to the beam tail. Self-consistent simulation results obtained with the particle-in-cell (PIC) code "WARP" [31] are shown in Sec. IV, confirming our expectations. Concluding remarks are finally made in Sec. V.

II. STOP-BAND DIAGRAM

A. Coherent and incoherent resonance conditions

It was pointed out over a half century ago that the betatron motion of a charged particle exposed to external periodic driving forces becomes unstable under the condition

$$k\nu_{0x} + \ell\nu_{0y} = n, \tag{1}$$

where (ν_{0x}, ν_{0y}) denote the *bare tunes* around the synchrotron, and (k, ℓ, n) are integers [32]. The driving potential of this resonance is proportional to $x^{|k|}y^{|\ell|}$ with (x, y) being the transverse spatial coordinates. The order of the resonance is $m = |k| + |\ell|$. This condition should be accurate if the effect of Coulomb interaction among individual particles is negligible.

The most common generalization of the single-particle resonance condition above, widely accepted in the community, is as follows:

$$k\nu_x + \ell\nu_y = n, \tag{2}$$

where (ν_x, ν_y) denote the *incoherent tunes* shifted from the bare tunes by the amount of $(\Delta\nu_x, \Delta\nu_y)$. The incoherent tune shifts $\Delta\nu_{x(y)} = \nu_{0x(0y)} - \nu_{x(y)}$, depending on which particle we observe, can be estimated by assuming some rigid distribution function. The concept of the incoherent resonance could approximately apply to particles in the beam tail (halo) because their Coulomb coupling with the beam's main body (core) is relatively weak. The core potential is only weakly affected by the presence of those tail particles, which means that they feel the core space-charge force as if it originates from an external source. This is basically why the *particle-core model* works to give an approximate description of mismatch-induced halo formation [33].

Unlike in the tail region, the correlation among the motions of individual particles is no longer negligible in the beam core. An accurate resonance criterion can be reached only by treating the core motion in a self-consistent manner. Even if a certain core particle fulfills the incoherent condition in Eq. (2), the betatron oscillation amplitude does not necessarily grow; the beam as a whole can maintain stability or no serious emittance growth occurs [34–36]. The core motion is essentially collective, so its stability is determined not by the incoherent oscillation of each single particle but by the coupled oscillations of all particles forming the core.

When the tune of a particular coherent oscillation mode is close to a half integer, the mode may become unstable. The two-dimensional (2D) coherent resonance condition, recently conjectured based on a one-dimensional (1D) Vlasov theory [37], can be expressed as

$$k(\nu_{0x} - C_m\Delta\bar{\nu}_x) + \ell(\nu_{0y} - C_m\Delta\bar{\nu}_y) = \frac{n'}{2}, \tag{3}$$

where n' is an integer, $(\Delta\bar{\nu}_x, \Delta\bar{\nu}_y)$ are the root-mean-squared (rms) tune shifts, and C_m is a positive constant depending on the resonance order m. The rms tune shifts are related to the rms tune depressions $\eta_{x(y)}$ as $\Delta\bar{\nu}_{x(y)} = (1 - \eta_{x(y)})\nu_{0x(0y)}$. These rms parameters, regarded as a measure of beam density in phase space, are evaluated from the rms envelope equations independently of the distribution function [38]. According to 1D Vlasov theories, the coherent tune-shift factor C_m is less than unity but gradually increases as the resonance order m becomes higher. A recent self-consistent numerical study has concluded that $C_2 \approx 0.7$, $C_3 \approx 0.8$, and $C_4 \approx 0.9$ [27]. These numbers shall be used in the following sections.

In a synchrotron consisting of N_{sp} lattice superperiods, the driving harmonic number n' on the right-hand side of Eq. (3) is replaced by $N_{\mathrm{sp}}n'$. The external fields (EF) produced, e.g., by nonlinear correction magnets can enhance the coherent instability of the same order but only with even n'.

The period of the core oscillation agrees with the lattice period unless the beam is strongly mismatched. Since the core space-charge potential acts as an external driving source to tail particles, the right-hand side of Eq. (2) should also be $N_{\mathrm{sp}}n'$ rather than n. Furthermore, we anticipate that tail-particle resonances are excited more seriously with even k and even ℓ, considering the spatial symmetry of the beam core focused by the quadratic AG potential. Particular attention should thus be required to the incoherent resonances under the condition

$$2k\nu_x + 2\ell\nu_y = N_{\mathrm{sp}}n' \tag{4}$$

with relatively small tune shifts $(\Delta\nu_x, \Delta\nu_y)$.

B. Beam-stability map

In general, the tune shifts $(\Delta\nu_x, \Delta\nu_y)$ become greater for particles closer to the center of the beam core. The incoherent tunes of individual particles then spread over a finite area in ν_{0x}-ν_{0y} plane, depending on the beam density and distribution function. The area covered by the incoherent tune spread is named "necktie" after its shape.

The original purpose of the so-called "necktie diagram" was to foresee most preferable operating tunes with which one could avoid possible resonance-induced beam loss. Such information is vital in the conceptual design stage of any circular machine. If the incoherent resonance condition in Eq. (2) really applies to the whole beam, the machine working point must be chosen such that the necktie does not cross any low-order single-particle resonance lines defined by Eq. (1).

As remarked above, the basic resonance mechanisms of a space-charge-dominated beam well matched to the machine lattice should be classified into two main categories, namely, the coherent resonance in the beam core and incoherent resonances of tail particles. The condition of the former resonance is given by Eq. (3) and the latter by Eq. (2) or (4). On the basis of this understanding, we proposed a new type of stability tune diagram free from the necktie concept [27,29]. A couple of examples corresponding to the lattice condition of the J-PARC Main Ring (MR) are exhibited in Fig. 1. The MR has a three-fold symmetric structure ($N_{\mathrm{sp}} = 3$) with correction sextupoles inserted in every lattice superperiod. The horizontal and vertical rms tune depressions are assumed to be equal, i.e., $\eta_x = \eta_y (\equiv \eta)$. The rms emittances in the two transverse directions are also roughly equal, which strongly suppresses the linear difference resonance along $\nu_{0x} - \nu_{0y} = 0$ (dashed line) [27]. The original operating point of the MR was moved to $(\nu_{0x}, \nu_{0y}) = (21.35, 21.43)$ in 2016 after the intensity upgrade [26]. This new operating point is located within the largest resonance-free area shown in Fig. 1(a).

A stop-band diagram as in Fig. 1 can readily be constructed for any circular lattice in the following way [29]. We first draw low-order coherent resonance lines in

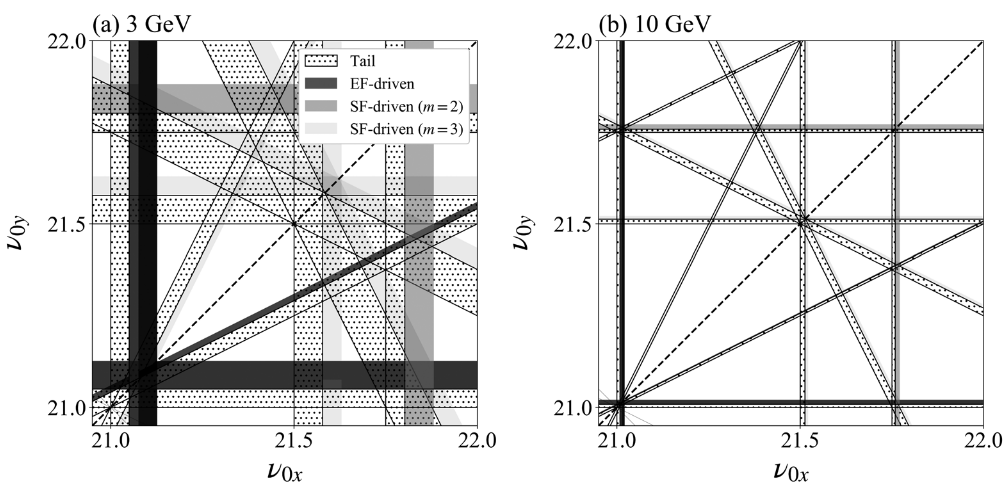

FIG. 1. Stop-band diagrams corresponding to the current operating condition of the J-PARC MR. The rms tune depression is estimated to be (a) $\eta \approx 0.994$ at 3 GeV and (b) $\eta \approx 0.999$ at 10 GeV. The coherent resonance bands of up to the third-order ($m \leq 3$) are plotted on the basis of Eq. (3) with $C_2 = 0.7$ and $C_3 = 0.8$. The third-order resonance driven by the normal sextupole magnets for orbit correction overlaps with the second-order resonance slightly above $\nu_{0x} = 21$. The width of each stop band is defined by the approximate formula in Eq. (5). The safety factor $\zeta_{k\ell}$ is set equal to unity for all stop bands. We have ignored the effect of error fields that produce additional stop bands.

ν_{0x}-ν_{0y} plane, making use of Eq. (3). Attention should be paid to all coherent resonances of up to the third order ($m \leq 3$) at least. If the beam stays in the machine for a long period at relatively low energy or only very little emittance growth is tolerated, it is advisable to take care of the fourth-order's ($m = 4$) as well for safety, which automatically covers the potentially dangerous incoherent resonances [under the condition (4)] of up to the eighth order. A finite width $\delta\nu_{k\ell}$ is then given to each resonance line. It is, however, extremely difficult to make a good estimate of $\delta\nu_{k\ell}$ because it depends on the detailed lattice design and even the distribution function of the beam.

Applying the smooth approximation to the Vlasov prediction in Ref. [37], we derived a simple formula

$$\delta\nu_{k\ell} \approx 2\zeta_{k\ell} f_{k\ell}(1 - C_m)\frac{1-\eta}{\eta}\bar{\nu}_0 \tag{5}$$

that can be used for a quick initial estimate for the band width. Here, $\zeta_{k\ell}(\geq 1)$ is the safety factor, and the average $\bar{\nu}_0 = (\nu_{0x} + \nu_{0y})/2$ is taken, assuming a modest tune split. $f_{k\ell}$ is defined by

$$f_{k\ell} \equiv \frac{|\ell\varepsilon_x + k\varepsilon_y|}{|\ell|\varepsilon_x + |k|\varepsilon_y}, \tag{6}$$

where ε_x and ε_y are the horizontal and vertical rms emittances at injection. This factor reflects the fact that a particular difference resonance ($k\ell < 0$) can be almost eliminated by adjusting the initial emittance ratio to $\varepsilon_x/\varepsilon_y = |k/\ell|$ [27]. Equation (5) points out that the width of a higher-order stop band is narrower. Since C_m approaches unity as the m number increases, it becomes more and more difficult to detect the instability of a highly nonlinear mode even if it is not Landau damped. The self-inhibition mechanism mentioned later also prevents us from identifying a clear signature of nonlinear-mode excitation.

In addition to the coherent core instability, we need to avoid incoherent resonances in the beam tail. The condition in Eq. (4) indicates that each coherent resonance band may be accompanied by incoherent tail resonances of twice the order. In fact, the coherent condition in Eq. (3) can be rewritten as $2k(\nu_{0x} - C_m\Delta\bar{\nu}_x) + 2\ell(\nu_{0y} - C_m\Delta\bar{\nu}_y) = N_{\rm sp}n'$. Since C_m is near unity (except for the dipole mode), this line is located close to the incoherent resonance line of the order $2m(= 2|k| + 2|\ell|)$ defined by Eq. (4). The incoherent tune shifts $\Delta\nu_{x(y)}$ of tail particles are generally not so large as the rms shift $\Delta\bar{\nu}_{x(y)}$. The region of possible tail resonances, therefore, lies below the lower boundary of each coherent resonance band as illustrated in Fig. 1. Franchetti, Métral *et al.* have discussed a similar feature of beam instabilities in the vicinity of a single-particle resonance line [39,40]. They found two distinct instability regimes lying side by side, one of which yields continuous particle losses and the other only emittance blowup with no significant losses.

The coherent tune-shift factor C_m of a higher-order mode is closer to unity, which makes the band width $\delta\nu_{k\ell}$ narrower. Moreover, the coherent core instability has a self-inhibition mechanism; weak nonlinear resonance automatically ceases to develop before leading to a well-detectable level of beam loss because the resonance-induced emittance growth reduces the beam density, thus resulting in the shift and shrinkage of the stop band. High-precision emittance measurement is usually required to find out the coherent resonance band if it exists. On the other hand, the betatron amplitudes of the tail particles captured by the incoherent resonance will keep growing until they hit the chamber wall. We suspect that most of beam losses observed in operating synchrotrons may be due to the incoherent effect in the beam tail.

The coherent resonance condition (3) together with the band-width formula (5) defines an approximate total width of each noncoupling instability band that includes the coherent core and incoherent tail resonance regions. As the coherent band shift is $C_m\Delta\bar{\nu}$ with $\Delta\bar{\nu}$ denoting either $\Delta\bar{\nu}_x$ or $\Delta\bar{\nu}_y$, the upper boundary of the stop band is distanced from the adjacent single-particle resonance line by $C_m\Delta\bar{\nu} + \delta\nu_m/2(\equiv w_m)$ with the coherent band width $\delta\nu_m = 2(1 - C_m)\Delta\bar{\nu}/\eta$. If η is not too far from unity, w_m is roughly equal to $\Delta\bar{\nu}$ independently of the resonance order m. Note that the extent of the Gaussian necktie is about twice as large as $\Delta\bar{\nu}$.

It is currently believed that the coherent instability of a nonlinear mode is hardly detectable (unless driven by external fields) or likely Landau-damped in a Gaussian beam. Even if so, the new stability map is still useful as it predicts the approximate boundaries of the regions where SF-driven incoherent resonances may occur in the beam tail. Major incoherent particle losses could be avoided by putting the operating point above the line defined by Eq. (3). This is a somewhat conservative criterion, but at least, more accurate than the conventional design guideline based on the necktie.

We stress the point that the proposed stability map is invented to show where in the tune space an intense hadron beam may become unstable due to possible resonant instabilities, even though it is well matched to the lattice at the beginning. Complicated transient phenomena during, e.g., beam injection and accumulation are outside the scope of the resonance-band theory. The purpose of our stability map is the same as the original purpose of the necktie diagram, that is, predicting the best machine operating region in the tune space. We are not very interested in identifying, *after* something bad happened under actual complicated experimental conditions of a particular machine, which single-particle resonance lines are responsible for the observed beam loss.

C. Overlapping resonances above a quarter-integer tune

Theoretically, the noncoupling resonance of the mth order always overlaps with the $2m$th-order's as is obvious from the resonance conditions. It does not matter whether the instability is coherent or incoherent. The overlapping of the coherent dipole ($m = 1$) instability with the coherent quadrupole ($m = 2$) instability has been experimentally confirmed by means of the "Simulator of Particle Orbit Dynamics" (S-POD), a novel tabletop ion-trap apparatus that provides a multi-particle Coulomb system physically equivalent to an intense relativistic beam in a large-scale accelerator [6]. It is rather easy to separate these two low-order modes because, firstly, the coherent dipole resonance is quite strong leading to the complete loss of the whole bunch once excited, secondly, the tune-shift factor C_1 is very different from those of other higher-order modes and, thirdly, the band width of the dipole instability is narrow.

In the vicinity of a quarter-integer tune, we have a possibility of the second-order ($m = 2$) and fourth-order ($m = 4$) coherent core resonances plus the fourth-order incoherent tail resonances. Such multiple resonance overlapping is also possible, in principle, for higher-order nonlinear modes. For instance, we expect a third-order ($m = 3$) coherent stop band partially overlapped with a narrow sixth-order's ($m = 6$), though the latter highly nonlinear core instability is probably undetectable. We would, however, be able to detect the six-order incoherent effect in the beam tail because it eventually causes some particle losses. Recent experimental results have even shown clear signatures of incoherent space-charge-driven resonances of the eighth order [41,42].

Figure 2 shows the stop-band diagram near a quarter-integer cell tune when η is fixed at 0.9 in both transverse directions. The difference resonance along the dashed line is deactivated because of the assumption that $\varepsilon_x = \varepsilon_y$. Two coherent resonance bands of $m = 2$ and 4 have overlapped. The fourth-order band is much narrower due to the C_4 factor closer to unity than C_2. It is positioned near the high-tune side of the second-order coherent band because the magnitude of the band shift $C_4\Delta\bar{\nu}$ is greater than $C_2\Delta\bar{\nu}$. The diagram in Fig. 2 tells that no severe emittance growth will occur in the region $\nu_{0x(0y)} > 1/4 + \Delta\bar{\nu} \approx 0.28$.

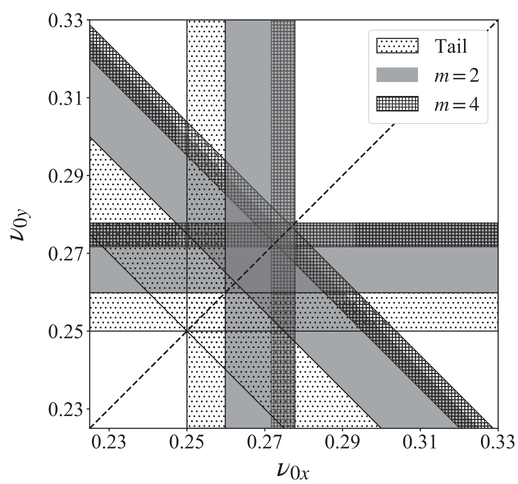

FIG. 2. Stop-band diagram near the cell tune of 0.25 (the betatron phase advance of 90°) under the condition $\varepsilon_x = \varepsilon_y$. The rms tune depression is assumed to be 0.9 everywhere in the diagram.

It should be informative to comment on the maximum incoherent tune spread, in other words, the size of the necktie. At the beam density considered here, $\max(\Delta\nu_{x(y)})$ is nearly 0.05, which means that, according to the conventional design criterion, the operating bare tune must be chosen above 0.30 in order to avoid resonant beam loss. As demonstrated later, this is clearly an overestimation; the actual band width is much narrower and closer to the above-mentioned coherent estimate, i.e., $\Delta\bar{\nu} \approx 0.03$.

III. TAIL SEPARATION

Tail particles execute the betatron oscillations with large amplitudes in full phase space, four-dimensional (4D) in the present case. Their oscillation energies are relatively large compared with those of core particles. The information necessary to identify outermost particles in phase space can be obtained from the Hamiltonian. Recalling the fact that the Coulomb potential energy is not so large in a synchrotron (accordingly, the tune depression is always near unity), we here consider the contribution from the linear space-charge terms only. The approximate Hamiltonian can then be written with the action variables $J_{x(y)}$ as

$$H = \frac{J_x}{\beta_x} + \frac{J_y}{\beta_y}, \tag{7}$$

where $\beta_{x(y)}$ denote the modified betatron functions calculated from the rms envelope equations with space charge [38]. The actions of a certain single particle at the canonical coordinates (x, y, p_x, p_y), including the influence of the space-charge potential, are evaluated from

$$2J_x = \beta_x p_x^2 + 2\alpha_x x p_x + \gamma_x x^2, \tag{8}$$

$$2J_y = \beta_y p_y^2 + 2\alpha_y y p_y + \gamma_y y^2, \tag{9}$$

where $\alpha_{x(y)}$ and $\gamma_{x(y)}$ are the Courant-Snyder functions derived easily from the space-charge-modified $\beta_{x(y)}$. Taking the average of Eq. (7) over a lattice superperiod or around the ring, we introduce the parameter

$$E \equiv \eta_x \nu_{0x} J_x + \eta_y \nu_{0y} J_y \tag{10}$$

that can be used as a measure of the approximate amplitude of a single-particle oscillation in 4D space. This simplified formula should be acceptable unless $\eta_{x(y)}$ is too far from unity.

In WARP simulations, we check the E-values of individual particles at injection to separate the contribution from large-amplitude particles to the rms emittance. Those tail particles defined at the entrance are excluded from the emittance evaluation thereafter, which clarifies whether the emittance of the core part grows or keeps the initial level. The rms emittance growth at the exit of the Nth cell is defined as

$$\Delta\varepsilon^{(\kappa)}(N) \equiv \frac{\varepsilon^{(\kappa)}(N) - \varepsilon^{(\kappa)}(0)}{\varepsilon^{(0)}(0)} \times 100[\%], \qquad (11)$$

where ε is the sum of the horizontal and vertical rms emittances. The index κ stands for the percentage of outermost particles marked initially and disregarded in the emittance evaluation; for instance, the calculation of $\varepsilon^{(20)}$ uses eighty percent of all particles.

IV. SIMULATION RESULTS

PIC simulations with the WARP code were carried out to explore the beam behavior in the vicinity of a quarter-integer cell tune. We used the Gaussian-type distribution initially matched the FD lattice including the Debye screening effect [43]. The matching is satisfactory especially in a relatively low beam-density range ($\eta = 0.9$) assumed here. The emittance growth induced by an initial mismatch is negligible, which enables us to identify a signature of even very weak instability.

For the sake of simplicity, the horizontal and vertical bare tunes were set equal; namely, $\nu_{0x} = \nu_{0y} (\equiv \nu_0)$. Figure 3 depicts the tune dependence of emittance growth after the beam passed through 100 cells, 200 cells and 1000 cells. The rms tune depressions are adjusted to 0.9 in both transverse directions as in the case of Fig. 2. We realize that the band width within which significant emittance growth has occurred is much narrower than the maximum extent of the Gaussian necktie that is roughly 0.05 in the present case (see, e.g., Fig. 8). The vertical lines in the picture indicate the approximate boundaries of the two coherent resonance regions. The incoherent tail resonances are expected just above the single-particle resonance line ($0.250 < \nu_0 \lesssim 0.260$), while the coherent core resonances of the second and fourth orders occur within the ranges $0.260 \lesssim \nu_0 \lesssim 0.278$ and $0.272 \lesssim \nu_0 \lesssim 0.278$, respectively, according to the stop-band diagram in Fig. 2.

Three curves in each panel of Fig. 3 are obtained from somewhat different ensembles of particles selected initially with the truncation factors $\kappa = 0\%$, 10%, and 20%. The emittance growth in the tail-resonance region can be eliminated almost completely by disregarding only 10–20% of outermost particles in 4D phase space; the emittance growth below ν_0 of around 0.26 is caused solely by the tail part

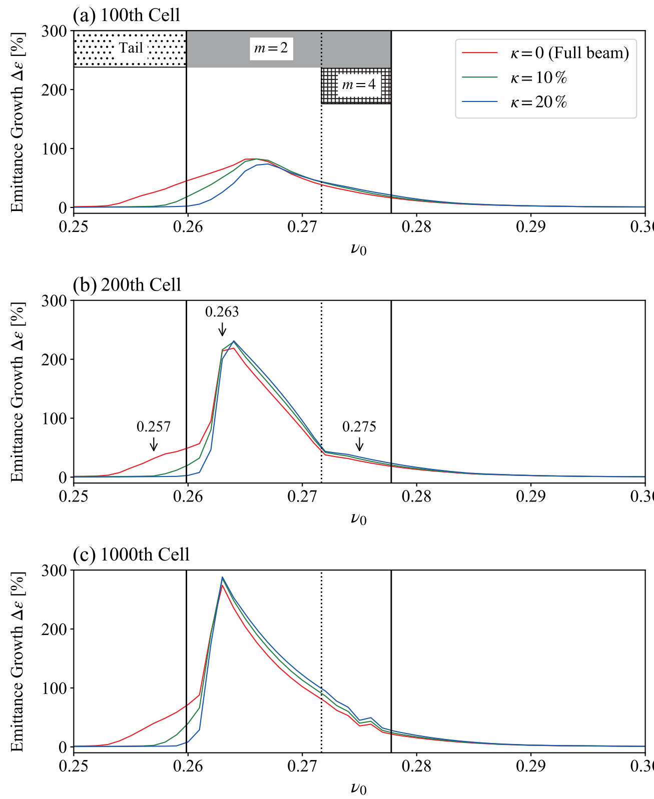

FIG. 3. Emittance growth of a Gaussian beam propagating through a long AG transport channel. The transport distances are (a) 100 FD cells, (b) 200 FD cells, and (c) 1000 FD cells. The rms tune depression is fixed at 0.9 regardless of the operating cell tune ν_0. Vertical lines show the boundaries of the second-order ($m = 2$) and fourth-order ($m = 4$) coherent resonance bands estimated from Eqs. (3) and (5) with $C_2 = 0.7$ and $C_4 = 0.9$. The phase-space configurations at the three operating tunes indicated by arrows in the middle picture are exhibited in Figs. 4–6.

separable from the core part. In striking contrast, the κ-dependence of the growth rate is weak inside the predicted core-resonance domain (between the vertical solid lines). These facts imply that the resonance mechanisms below and above $\nu_0 \approx 0.26$ differ essentially.

A. Phase-space configurations

Typical phase-space configurations in the tail-resonance region ($\nu_0 = 0.257$), the second-order core-resonance band ($\nu_0 = 0.263$), and the fourth-order core-resonance band ($\nu_0 = 0.275$), are plotted in Figs. 4–6. The abscissa ($\tilde{x}$) and ordinate ($\tilde{p}_x$) in these figures are scaled to be dimensionless; specifically, we have divided the horizontal canonical variables (x, p_x) by their rms averages at the entrance. The color of each macroparticle is chosen depending on the initial E-value, and kept unchanged until the transport exit. The color varies from red to blue as the initial energy increases.

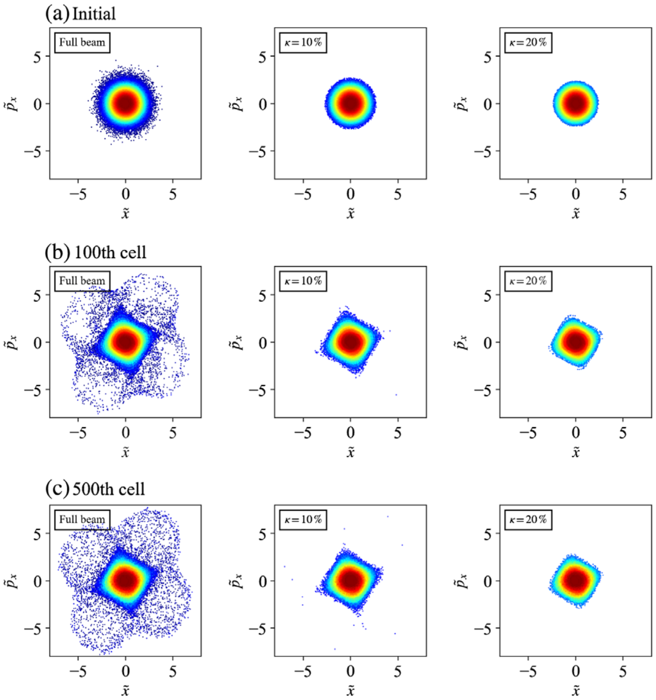

FIG. 4. Phase-space configurations at $\nu_0 = 0.257$ with three different tail-truncation factors ($\kappa = 0, 10, 20$), observed at (a) the transport entrance, (b) 100th FD cell, and (c) 500th FD cell.

At $\nu_0 = 0.263$ around which most severe emittance growth has occurred, the fourth-order resonance is excited first in the beam tail, followed by much stronger instability that completely destroys the core (Fig. 5). A clear two-arm structure is developed in phase space, indicating the instability of the second-order mode. Note that the final distributions obtained with three different κ-factors look nearly identical.

The phase-space profile at $\nu_0 = 0.257$ (Fig. 4) in the tail-resonance region is obviously different from what we found in Fig. 5. The core is almost unaffected throughout the transport channel (except for a slight distortion of its boundary), but on the other hand, a large halo is formed around it. It is apparent from Fig. 4 that only about 10% of particles with high initial energies contribute to the halo formation, which is why the rms emittance growth at $\nu_0 = 0.257$ disappears with $\kappa = 10\%$ in Fig. 3.

A question now is whether we see an analogous beam behavior around $\nu_0 = 0.275$ where the resonance of the same order as at $\nu_0 = 0.257$ is expected theoretically. Although both resonances below the lower boundary (Fig. 4) and near the upper boundary (Fig. 6) of the core instability band are of the fourth order, we recognize a substantial disparity between them. Unlike the case of Fig. 4 where the core maintains the initial configuration, a four-island structure has been formed at $\nu_0 = 0.275$ (Fig. 6) inside the core with almost no tail expansion as observed in Fig. 4. We also notice that many particles initially located around the core center have spread all over but their amplitudes are bounded within a relatively narrow area comparable to the initial core size. Even if we increase the κ-factor, the rms emittance still grows similarly in time at $\nu_0 = 0.275$ as shown in Fig. 7(c). The time evolution of the

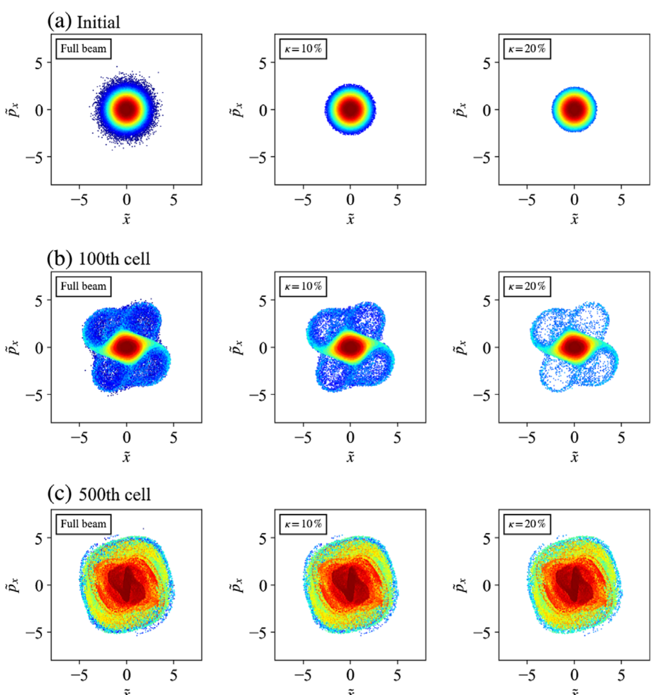

FIG. 5. Phase-space configurations at $\nu_0 = 0.263$ with three different tail-truncation factors ($\kappa = 0, 10, 20$), observed at (a) the transport entrance, (b) 100th FD cell, and (c) 500th FD cell.

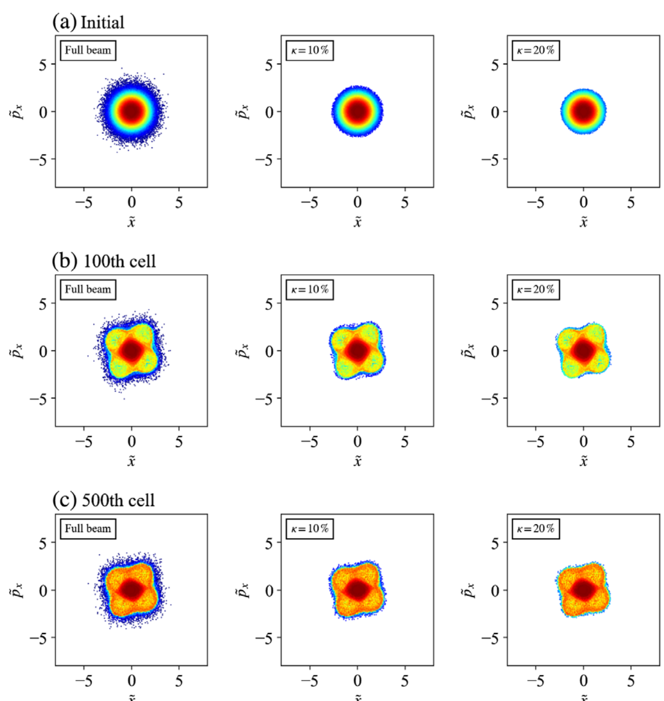

FIG. 6. Phase-space configurations at $\nu_0 = 0.275$ with three different tail-truncation factors ($\kappa = 0, 10, 20$), observed at (a) the transport entrance, (b) 100th FD cell, and (c) 500th FD cell.

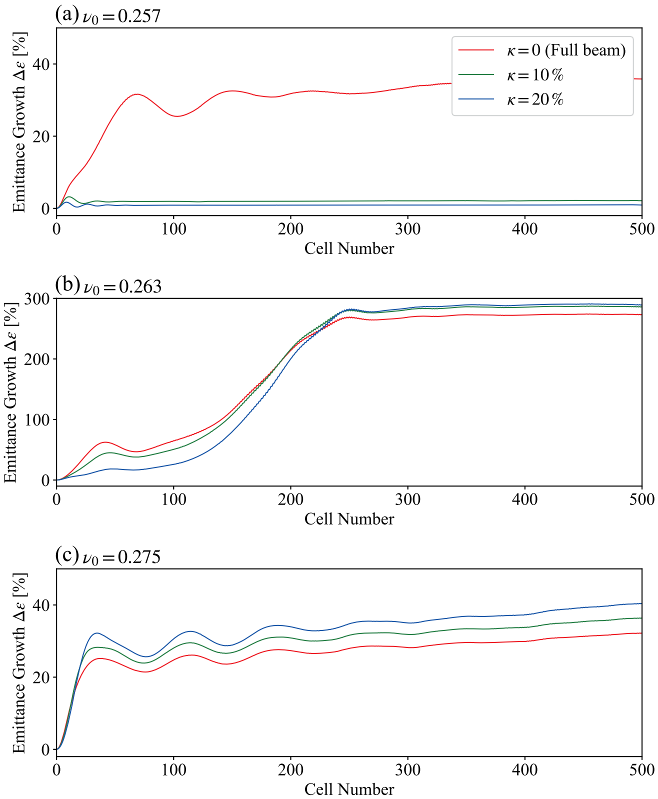

FIG. 7. Time evolution of the rms emittance-growth rates in the three cases of Figs. 4–6. The operating bare tune per cell is fixed at (a) $\nu_0 = 0.257$, (b) $\nu_0 = 0.263$, and (c) $\nu_0 = 0.275$.

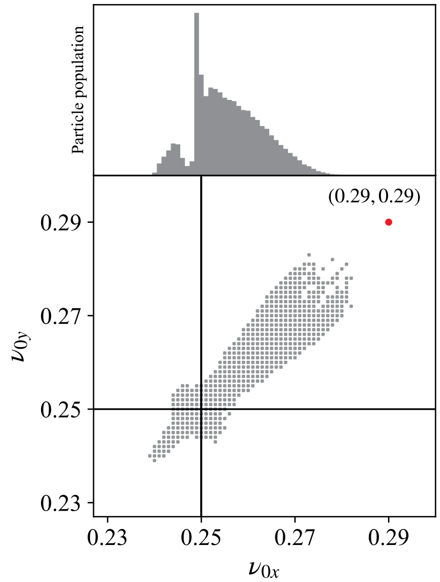

FIG. 8. Incoherent tune spread of a Gaussian beam at $\nu_{0x} = \nu_{0y} = 0.290$ (red dot) where the emittance growth is negligible. The rms tune depression is adjusted initially to $\eta = 0.9$, the same as in the case of Fig. 3.

emittance growth at $\nu_0 = 0.263$ is also insensitive to the κ-factor [Fig. 7(b)]. In both Figs. 5 and 6, the final phase-space configurations in the lower three panels look more or less similar. In contrast, significant κ-dependence can be seen in the beam profiles displayed in Fig. 4(c).

B. Incoherent-tune spectra

The numerical observations in the last subsection strongly suggest that the resonances at $\nu_0 = 0.263$ and 0.275 belong to the same family. The fundamental mechanism of instability at $\nu_0 = 0.257$ is different from the other two. This interpretation is consistent with the resonance theory and diagram discussed in Sec. II. According to the proposed theory, the former two at $\nu_0 = 0.263$ and 0.275 are the coherent effect in the core while the latter at $\nu_0 = 0.257$ the incoherent effect in the beam tail. A signature of the possible fourth-order coherent mode excitation has been observed even experimentally in the S-POD system [42].

Above the upper boundary of the coherent band ($\nu_0 \gtrsim 0.28$), no resonant instability to which one must pay serious attention has occurred; only negligible emittance growth is observed in spite of the core deformation as depicted in Fig. 8. In this example, the operating tune is adjusted to 0.290 beyond the predicted coherent instability band. The necktie has been distorted around the point $(\nu_{0x}, \nu_{0y}) = (0.25, 0.25)$, but only limited rms emittance growth (less than a few percent over 1000 cells) occurs as is evident from Fig. 3. Such distortion of an incoherent tune spread around single-particle resonance lines has been repeatedly observed in past PIC simulations [27,29,30]. Even if core particles with large incoherent tune shifts exactly satisfy the condition in Eq. (2), no severe emittance growth occurs as long as the operating point is put outside the coherent resonance band. In a practical sense, therefore, we do not have to care about the tune-spectrum distortion like Fig. 8 that happens in the range $\nu_0 \gtrsim 1/4 + \Delta\bar{\nu}$.

For comparison, we show in Fig. 9 the incoherent-tune distribution when the operating point is set at $\nu_0 = 0.275$ in the middle of the fourth-order core resonance band. The incoherent tunes are evaluated by Fourier analyzing the orbits of individual particles after the initial beam instability was more or less settled; the tune spectrum is obtained based on the orbit data from 300th cell to 1300th cell. What we see in Fig. 9 is a sort of consequence after the particles were redistributed due to the core instability. The upper panel indicates that a lot of particles originally positioned well below the line $\nu_{0x(0y)} = 1/4$ got unstable and eventually populated around or above it. A similar phenomenon also takes place when the beam is captured by a different type of nonlinear coherent resonance. See the Appendix for the case where the operating point is chosen within a coherent parametric resonance band of the third order.

The influence of the linear coherent instability upon the core is surely more destructive than the fourth-order effect. As illustrated in Fig. 7(b), the development of the strong

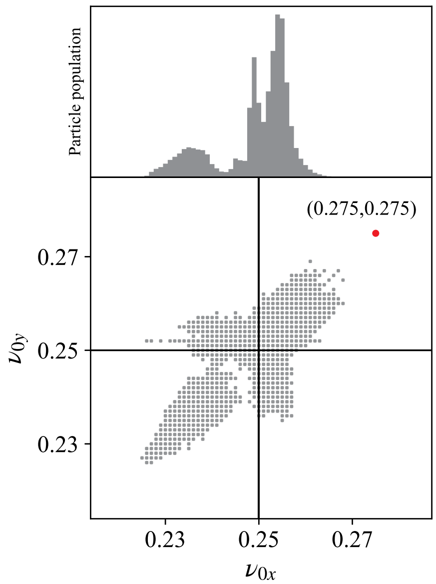

FIG. 9. Incoherent tune spread of a Gaussian beam after the rapid initial emittance growth due to the fourth-order resonance was nearly settled. The operating point is set at $\nu_{0x} = \nu_{0y} = 0.275$ (red dot) where non-negligible emittance growth occurs. The rms tune depression is adjusted initially to $\eta = 0.9$.

core instability is settled after around the 300th FD cell at which the emittance growth has reached about 300%. The Fourier analysis of the betatron orbits of individual particles in this final state results in Fig. 10; it turns out that almost all particles are moved above $\nu_{0x(0y)} = 1/4$ in tune space,

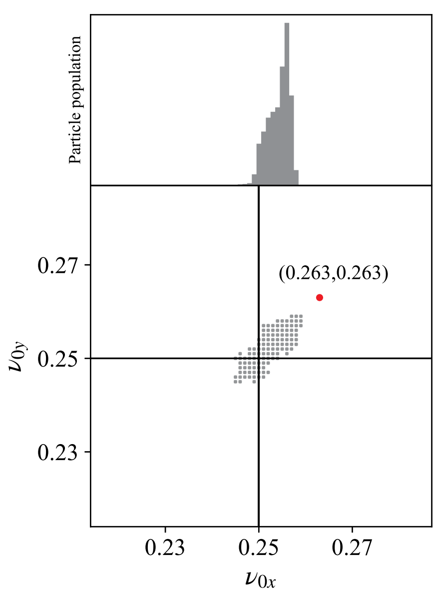

FIG. 10. Incoherent tune spread of a Gaussian beam at $\nu_{0x} = \nu_{0y} = 0.263$ (red dot) where the severe coherent envelope instability is expected. The conditions of the PIC simulation and Fourier analysis are the same as adopted in Fig. 9 (except for the operating bare tunes).

forming a sharp peak. Unlike in the case of nonlinear coherent resonances, no small second mountain below $\nu_{0x(0y)} = 1/4$ remains. The core is completely destroyed and the resultant large emittance growth reduces the beam's phase-space density considerably, making the tune spread much narrower than the original size (~0.05).

In any case, even if many particles were eventually accumulated near or above $\nu_{0x(0y)} = 1/4$, it does not necessarily mean that the incoherent mechanism is responsible for the collapse of the initial beam distribution. Recalling the tune-spread profile at the entrance, we understand that major instability was initiated in Figs. 9 and 10 not on the line $\nu_{0x(0y)} = 1/4$ but well below it, kicking many particles out of the original core. A piece of related information is given in Appendix.

V. CONCLUDING REMARKS

We have conducted a detailed study about the so-called "90° stop band" potentially dangerous at high beam density not only in linacs but also in circular hadron machines. Self-consistent numerical simulations were performed to clarify the resonance feature above the betatron phase advance of 90° per unit AG cell. The resonance theory recently proposed in Refs. [27] and [29] was applied to explain the numerical observations. The present results suggest the existence of three different types of resonances; in addition to the linear coherent resonance (envelope instability) in the beam core, the coherent and incoherent resonances of the fourth order will be encountered within the 90° stop band.

The coherent fourth-order stop band is located near the upper boundary of the instability region whose total width is given approximately by $\Delta\bar{\nu}$ (provided no external driving force exists). The incoherent fourth-order stop band lies just above the single-particle resonance line $\nu_{0x(0y)} = 1/4$ because this type of resonance is effective only in the beam tail where the incoherent tune shift of each particle is relatively small. The unstable particles captured by the incoherent resonances are only a minor portion of the whole beam and separable from the other part, which is not the case with the coherent core resonances. The core stability is not seriously affected by the incoherent mechanism as expected from self-consistent theories. The new stop-band diagram appears to be consistent with the PIC simulation data. No severe emittance growth occurs outside the predicted instability band of the width $\Delta\bar{\nu}$ (much narrower than the maximum incoherent tune spread of the Gaussian beam) even though many core particles are sitting exactly on the neighboring incoherent resonance lines. Caution should be demanded when the conventional necktie is used for the conceptual design of a high-intensity circular lattice.

Similar multiple resonance overlapping is theoretically possible for higher orders as well, but highly nonlinear coherent modes are weak (or simply Landau-damped) and even deactivated spontaneously. The incoherent resonance mechanism in the beam tail will then play a more important role from a practical point of view. A core resonance band of higher order is narrower and has a larger shift from its adjacent single-particle resonance line, which expands the tail-resonance region. In many cases, therefore, beam losses in operating synchrotrons could be linked more closely to the incoherent tail effect [44]. If this is really the case, we may be able to broaden the usable operating region in the tune space by controlling the tail loss somehow. In the case of Fig. 3, for example, the emittance growth and resultant beam loss in the tail-resonance region ($\nu_0 \lesssim 0.26$) will be suppressed if we inject a hard-edged beam. Such broadening of the stability area has been confirmed in past PIC simulations with the waterbag and parabolic distributions [27].

The phase-space configuration of any real beam is not the precise Gaussian as considered here but often deviated from the Gaussian profile especially after complicated injection procedures. In the 3-GeV rapid cycling synchrotron at J-PARC, the sophisticated injection painting scheme has been employed to form a non-Gaussian beam intentionally for space-charge mitigation; the real-space profile of the accumulated long bunch is roughly uniform in the longitudinal direction and near-parabolic in the transverse [45,46]. Holmes *et al.* proposed the formation of a hard-edged beam by means of the painting [47]. We believe that these attempts must be beneficial for minimizing the beam loss of tail origin, thus somewhat widening the stable operating area in tune space.

APPENDIX: INCOHERENT TUNE DISTRIBUTION OF A WATERBAG BEAM CAPTURED BY A COHERENT PARAMETRIC RESONANCE OF THE THIRD ORDER

The coherent resonance condition in Eq. (3) predicts the possibility of the third-order ($m = 3$) noncoupling instability slightly above the line $\nu_{0x(0y)} = 1/6$. Figure 11 shows a typical WARP result obtained at $\nu_0 = 0.192$ with an initially matched waterbag beam. The core has been deformed into a trianglelike shape, which indicates the excitation of the third-order resonance as expected. This can never be the incoherent effect because the conventional condition in Eq. (2) only predicts the sixth-order resonance near the bare tune of 1/6.

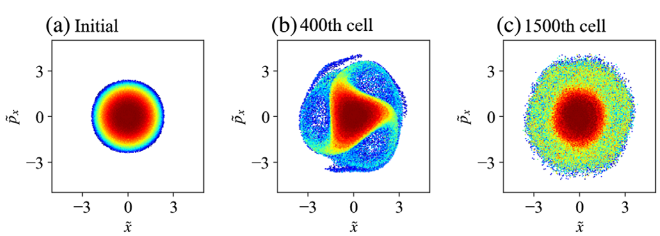

FIG. 11. Horizontal phase-space configurations of a waterbag beam observed at (a) the transport entrance, (b) 400th FD cell, and (c) 1500th FD cell. The initial rms tune depression is chosen to be $\eta = 0.8$. The operating point is set at $\nu_{0x} = \nu_{0y} = 0.192$ where the coherent sextupole ($m = 3$) parametric resonance is expected from Eq. (3).

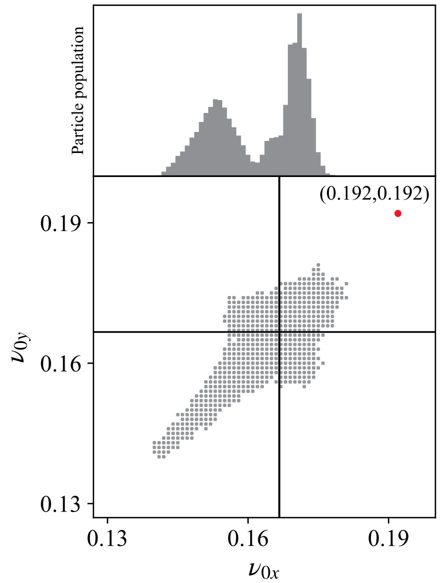

FIG. 12. Incoherent tune spread of the waterbag beam exhibited in Fig. 11, after the initial particle distribution collapsed due to the coherent core resonance. The vertical and horizontal solid lines in the lower panel represent $\nu_{0x(0y)} = 1/6$.

In this example, the rms emittance starts to grow rapidly at around 300th FD cell and comes into a sort of plateau after around 600th cell where the emittance growth of roughly 70% is reached. The incoherent tunes of individual particles, calculated from their betatron orbits between 500th and 1500th cell, are plotted in Fig. 12. Similarly to the fourth-order case in Fig. 9, many core particles move to the high-tune side, forming a peak near the line $\nu_{0x(0y)} = 1/6$ (though the initial instability was definitely the third-order coherent).

[1] H. Hotchi, H. Harada, N. Hayashi, S. Kato, M. Kinsho, K. Okabe, P. K. Saha, Y. Shobuda, F. Tamura, N. Tani, Y. Watanabe, K. Yamamoto, M. Yamamoto, and M. Yoshimoto, Achievement of a low-loss 1-MW beam operation in the 3-GeV rapid cycling synchrotron of the Japan Proton Accelerator Research Facility, Phys. Rev. Accel. Beams **20**, 060402 (2017).

[2] N. Madsen, P. Bowe, M. Drewsen, L. H. Hornekær, N. Kjærgaard, A. Labrador, J. S. Nielsen, J. P. Schiffer, P. Shi, and J. S. Hangst, Density Limitation in a Stored Laser-cooled Ion Beam, Phys. Rev. Lett. **83**, 4301 (1999).

[3] H. Okamoto, Y. Wada, and R. Takai, Radio-frequency quadrupole trap as a tool for experimental beam physics, Nucl. Instrum. Methods Phys. Res., Sect. A **485**, 244 (2002).

[4] H. Okamoto, M. Endo, K. Fukushima, H. Higaki, K. Ito, K. Moriya, S. Yamaguchi, and S. M. Lund, Experimental simulation of beam propagation over long path lengths using radio-frequency and magnetic traps, Nucl. Instrum. Methods Phys. Res., Sect. A **733**, 119 (2014).

[5] K. Moriya, K. Fukushima, K. Ito, T. Okano, H. Okamoto, S. L. Sheehy, D. J. Kelliher, S. Machida, and C. R. Prior, Experimental study of integer resonance crossing in a nonscaling fixed field alternating gradient accelerator with a Paul ion trap, Phys. Rev. ST Accel. Beams **18**, 034001 (2015).

[6] K. Moriya, M. Ota, K. Fukushima, M. Yamaguchi, K. Ito, and H. Okamoto, Double stop-band structure near half-integer tunes in high-intensity rings, Phys. Rev. Accel. Beams **19**, 114201 (2016).

[7] K. Ito, H. Okamoto, Y. Tokashiki, and K. Fukushima, Coherent resonance stop bands in alternating gradient beam transport, Phys. Rev. Accel. Beams **20**, 064201 (2017).

[8] N. Christofilos, Focusing system for ions and electrons, US patent No. 2736799, 1950.

[9] E. D. Courant, M. S. Livingston, and H. S. Snyder, The strong-focusing synchrotron—A new high energy accelerator, Phys. Rev. **88**, 1190 (1952).

[10] *Handbook of Accelerator Physics and Engineering*, edited by A. W. Chao and M. Tigner (World Scientific, Singapore, 1999).

[11] H. Wiedemann, *Particle Accelerator Physics* (Springer-Verlag, New York, 1993).

[12] M. Reiser, *Theory and Design of Charged Particle Beams* (John Wiley & Sons, New York, 2008) and references therein.

[13] I. Hofmann, L. J. Laslett, L. Smith, and I. Habor, Stability of the Kapchinskij-Vladimirskij (K-V) distribution in long periodic transport systems, Part. Accel. **13**, 145 (1983).

[14] J. Struckmeier and M. Reiser, Theoretical studies of envelope oscillations and its instabilities of mismatched intense charged-particle beams in periodic focusing channels, Part. Accel. **14**, 227 (1984).

[15] C. Chen and R. C. Davidson, Nonlinear Resonances and Chaotic Behavior in a Periodically Focused Intense Charged-Particle Beams, Phys. Rev. Lett. **72**, 2195 (1994).

[16] S. Y. Lee and A. Riabko, Envelope Hamiltonian of an intense charged-particle beam in periodic solenoidal fields, Phys. Rev. E **51**, 1609 (1995).

[17] S. M. Lund and B. Bukh, Stability properties of the transverse envelope equations describing intense ion beam transport, Phys. Rev. ST Accel. Beams **7**, 024801 (2004).

[18] C. Li and Y. L. Zhao, Envelope instability and the fourth order resonance, Phys. Rev. ST Accel. Beams **17**, 124202 (2014).

[19] L. Groening, W. Barth, W. Bayer, G. Clemente, L. Dahl, P. Forck, P. Gerhard, I. Hofmann, M. S. Kaiser, M. Maier, S. Mickat, T. Milosic, D. Jeon, and D. Uriot, Experimental Evidence of the 90° Stop Band in the GSI UNILAC, Phys. Rev. Lett. **102**, 234801 (2009).

[20] D.-O. Jeon, Experimental evidence of space charge driven resonances in high intensity linear accelerators, Phys. Rev. Accel. Beams **19**, 010101 (2016).

[21] A. V. Fedotov and I. Hofmann, Half-integer resonance crossing in high-intensity rings, Phys. Rev. ST Accel. Beams **5**, 024202 (2002).

[22] A. V. Fedotov, I. Hofmann, R. L. Gluckstern, and H. Okamoto, Parametric collective resonances and space-charge limit in high-intensity rings, Phys. Rev. ST Accel. Beams **6**, 094201 (2003).

[23] S. Cousineau, S. Y. Lee, J. A. Holmes, V. Danilov, and A. Fedotov, Space charge induced resonance excitation in high intensity rings, Phys. Rev. ST Accel. Beams **6**, 034205 (2003).

[24] T. Uesugi, S. Machida, and Y. Mori, Experimental study of a half-integer resonance with space-charge effects in a synchrotron, Phys. Rev. ST Accel. Beams **5**, 044201 (2002).

[25] T. Uesugi, T. Fujisawa, K. Noda, Y. Hashimoto, S. Machida, Y. Mori, and H. Uchiyama, Observation of beam-size blowup due to half-integer resonance in a synchrotron, Phys. Rev. ST Accel. Beams **7**, 064203 (2004).

[26] S. Igarashi *et al.*, Accelerator design for 1.3 MW beam power operation of the J-PARC Main Ring, Prog. Theor. Exp. Phys. **2021**, 033G01 (2021).

[27] K. Kojima, H. Okamoto, and Y. Tokashiki, Empirical condition of betatron resonances with space charge, Phys. Rev. Accel. Beams **22**, 074201 (2019).

[28] K. Kojima, H. Okamoto, and Y. Tokashiki, Reply to "Comment on 'Empirical condition of betatron resonances with space charge'", Phys. Rev. Accel. Beams **23**, 028002 (2020).

[29] H. Okamoto, M. Aoki, C. Ichikawa, K. Kojima, T. Kurauchi, and Y. Yamane, Coherent and incoherent space-charge effects in high-intensity hadron rings, J. Instrum. **15**, P07017 (2020).

[30] I. Hofmann, A. Oeftiger, and O. Boine-Frankenheim, Self-consistent long-term dynamics of space charge driven resonances in 2D and 3D, Phys. Rev. Accel. Beams **24**, 024201 (2021).

[31] D. P. Grote, A. Friedman, G. D. Craig, I. Haber, and W. M. Sharp, Progress toward source-to-target simulation, Nucl. Instrum. Methods Phys. Res., Sect. A **464**, 563 (2001).

[32] E. D. Courant and H. S. Snyder, Theory of alternating-gradient synchrotron, Ann. Phys. (N.Y.) **3**, 1 (1958).

[33] T. Wangler, *RF Linear Accelerators* (John Wiley & Sons, New York, 1998) and references therein.

[34] L. Smith, Effect of gradient errors in the presence of space charge forces, *Proceedings of the 4th International Conference on High-Energy Accelerators*, edited by A. A. Kolomenskij and A. B. Kuznetsov (Dubna, USSR, 1963), p. 1232.

[35] F. J. Sacherer, Ph.D thesis, Lawrence Radiation Laboratory, 1968; Report No. UCRL-18454, 1968.

[36] R. Baartman, Betatron resonances with space charge, in *Proceedings of Space Charge Physics in High Intensity Hadron Rings* (Shelter Island, New York, USA, 1998); Betatron resonances with space charge, AIP Conf. Proc. **448**, 56 (1998).

[37] H. Okamoto and K. Yokoya, Parametric resonances in intense one-dimensional beams propagating through a periodic focusing channel, Nucl. Instrum. Methods Phys. Res., Sect. A **482**, 51 (2002).

[38] F. J. Sacherer, Rms envelope equations with space charge, IEEE Trans. Nucl. Sci. **18**, 1105 (1971).

[39] G. Franchetti, I. Hofmann, M. Giovannozzi, M. Martin, and E. Metral, Space charge and octupole driven resonance trapping observed at the CERN Proton Synchrotron, Phys. Rev. ST Accel. Beams **6**, 124201 (2003).

[40] E. Métral, G. Franchetti, M. Giovannozzi, I. Hofmann, M. Martini, and R. Steerenberg, Observation of octupole driven resonance phenomena with space charge at the CERN Proton Synchrotron, Nucl. Instrum. Methods Phys. Res., Sect. A **561**, 257 (2006).

[41] F. Asvesta, H. Bartosik, S. Gilardoni, A. Huschauer, S. Machida, Y. Papaphilippou, and R. Wasef, Identification and characterization of high order incoherent space charge driven structure resonances in the CERN Proton Synchrotron, Phys. Rev. Accel. Beams **23**, 091001 (2020).

[42] T. Ikeda, K. Ito, and H. Okamoto, Novel tabletop experiment demonstrating the nonlinear resonance excitation observed at the CERN Proton Synchrotron, Jpn. J. Appl. Phys. **60**, 070901 (2021).

[43] S. M. Lund, T. Kikuchi, and R. C. Davidson, Generation of initial kinetic distributions for simulation of long-pulse charged particle beams with high space-charge intensity, Phys. Rev. ST Accel. Beams **12**, 114801 (2009).

[44] The coherent effect will be more important in a high-intensity injector linac where the beam is much denser in phase space.

[45] H. Hotchi (private communication).

[46] H. Hotchi, Effects of Montague resonance on the formation of the beam distribution during multiturn injection painting in a high-intensity proton ring, Phys. Rev. Accel. Beams **23**, 050401 (2020).

[47] J. A. Holmes, T. Gorlov, N. J. Evans, M. Plum, and S. Cousineau, Injection of a self-consistent beam with linear space-charge force into a ring, Phys. Rev. Accel. Beams **21**, 124403 (2018).